Strain-Induced Crystallization of Natural Rubber and Cross-Link Densities Heterogeneities

ARTICLE *in* MACROMOLECULES · AUGUST 2014

Impact Factor: 5.8 · DOI: 10.1021/ma5006843

Macromolecules

Article

pubs.acs.org/Macromolecules

Strain-Induced Crystallization of Natural Rubber and Cross-Link Densities Heterogeneities

Nicolas Candau,[†,‡] Rabia Laghmach,[‡,∥] Laurent Chazeau,[*,†,‡] Jean-Marc Chenal,[†,‡] Catherine Gauthier,[§] Thierry Biben,[∥] and Etienne Munch[§]

[†]Université de Lyon, CNRS, F-69621, Lyon, France

[‡]MATEIS, INSA-Lyon, CNRS UMR5510, F-69621, Lyon, France

[§]Centre de technologies, Manufacture Française des Pneumatiques Michelin, 63040 Clermont Ferrand Cedex 9, France

[∥]Institut Lumière Matière, UMR5306 CNRS, Université Claude Bernard Lyon 1, 69622 Villeurbanne Cedex, France

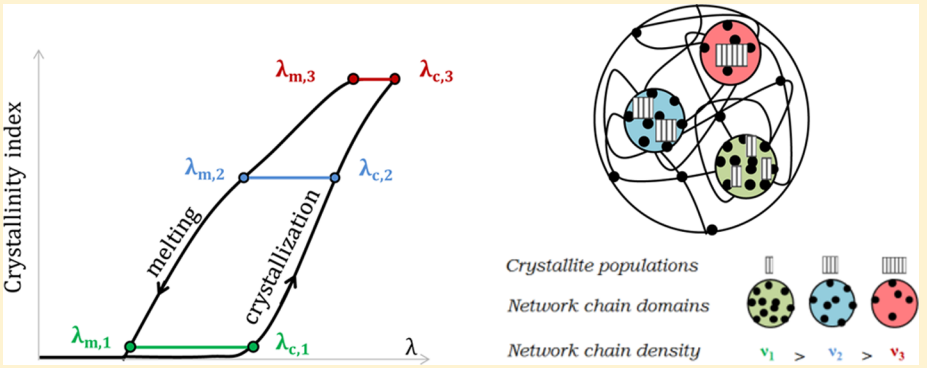

ABSTRACT: Strain-induced crystallization (SIC) of natural rubber (NR) is characterized during a cyclic deformation at room temperature and low strain rate ($\sim 10^{-3}$ s^{-1}) using in situ wide angle X-rays scattering (WAXS) measurements. The crystallinity index (CI) and average size of the crystallites in the three main directions are measured during loading and unloading. A scenario describing SIC is then proposed, assuming that SIC corresponds to the successive appearance of crystallite populations whose nucleation and growth depend on the local network density. From this scenario, a methodology, coupling experimental observations and thermodynamic description is developed to determine the distribution of the network chain density associated with the size of a corresponding crystallite population. Finally, complex cyclic tests are performed. They suggest the existence of a memory effect in the chains involved in crystallization, which eases the nucleation process of the crystallites.

1. INTRODUCTION

The ability of natural rubber (NR) to crystallize under strain is often said to be at the origin of its enhanced mechanical properties and particularly of its crack growth resistance[1−5] and fatigue behavior.[6−8] Thus, strain-induced crystallization (SIC) of NR has been widely studied since its discovery in 1925 by Katz,[9] and many theoretical descriptions,[10−14] experimental investigations,[15−23] and reviews[24,25] are available in the literature. SIC can be indirectly characterized by methods such as thermal measurements,[26−28] birefringence,[15] dilatometry,[29] or stress relaxation.[30] Moreover, its morphological features can be studied by electron microscopy (TEM)[31−35] and in situ wide-angle X-ray scattering (WAXS) experiments.[17,19,36−38] The aforementioned technique appears to be the most appropriate for understanding the mechanisms of SIC, as it gives significant information on the crystalline content, the crystallite size and their orientation. Besides, several thermodynamic models of strain-induced crystallization of natural rubber are proposed in the literature.[10−12,14,39] Nevertheless, few of these models are really connected to the analysis of the crystalline microstructure. The pioneering work in this domain is that of Flory.[12] The strength of his model lies in the fact that the crystallization is explicitly related to the mechanical response, and more specifically the relaxation of the amorphous phase, that has been evidenced experimentally.[18,30,38] Later, Flory's type models[10,11] accounted for the morphology of the crystals (folded or extended chains crystals). In these models, SIC is triggered by the density of the cross-linking nodes of the vulcanized NR. However, the vulcanized NR is depicted as an homogeneous material in all of these models, despite experimental evidence of its heterogeneous nature (studies based on SANS,[40,41] WAXS,[20,42] NMR[43,44] and thermoporosimetry[45] measurements). Homogeneous crystallization cannot correctly describe the influence of the network chain densities on this phenomenon. In particular, it has been extensively evidenced that the stretching ratio at crystallization onset λ_c, is around 4, regardless of the average network chain density (ν).[17,19,37] By assuming that the orientation of the

Received: April 2, 2014
Revised: July 22, 2014

   dx.doi.org/10.1021/ma5006843 | *Macromolecules* XXXX, XXX, XXX−XXX

chains governs the SIC process, such experimental results evidence that the local network density of the first chains involved in SIC does not differ much from a material to another. Thus, Tosaka[46] highlighted the importance of the heterogeneous nature of the vulcanized rubber. He considered the existence of two types of networks—one being responsible for rubber elasticity and the other one acting like a fluid mass—to describe the stress relaxation due to SIC.

However, some questions remain unsolved, namely: how to identify the domains of the material involved in the SIC process? How to quantify the length of the chains in these domains? This paper aims to address these open questions thanks to the experimental determination of the crystallinity index and average crystallite size measured during cyclic tests at relatively slow strain rate and the analysis of these data from thermodynamic description. A methodology is also proposed to quantify the distribution of the local network densities involved in SIC process as well as the distribution of the corresponding crystallite size. In addition, original cyclic experiments are performed above the melting stretching ratio to study the influence of the material crystallization history on its ability to recrystallize.

2. MATERIALS AND METHODS

2.1. Materials. A cross-linked unfilled NR, obtained by vulcanization of NR gum is considered in this work with the following recipe: rubber gum (100 phr) which is a Technically Specified Rubber (TSR20) provided by Michelin Tire Company, stearic acid (2 phr), ZnO (1.5 phr), 6PPD (3 phr), CBS (1.9 phr), and sulfur (1.2 phr) (where phr means g per 100g of rubber). The material has been processed following the Rauline patent.[47] First, the gum is introduced in an internal mixer and sheared for 2 min at 60 °C. Then, the vulcanization recipe is added and the mix is sheared for 5 min. Afterward, the material is sheared in an open mill for 5 min at 60 °C. Sample sheets are then obtained by hot pressing at 170 °C during 13 min. Dumbbell-shaped samples, with a 6 mm gauge length (l_0) and 0.8 mm thickness, are machined. The number density of the elastically effective subchains (so-called hereafter average network chain density ν) was estimated from the swelling ratio in toluene and from the Flory–Rehner equation[48] and found equal to 1.4×10^{-4} mol·cm^{-3}. The density is tuned so that (i) it is close to the optimum network density enhancing the development of strain-induced crystallization[17] and (ii) it is high enough to avoid the inverse yield effect,[18] an undesired phenomenon in slightly vulcanized rubbers. In order to avoid microstructure modification during the different mechanical tests, i.e., an uncontrolled Mullins effect, the samples are stretched four times up to stretching ratio ($\lambda = 7$) higher than the maximum stretching ratio reached during the in situ cyclic tests ($\lambda = 6$)

2.2. In Situ Waxs Analysis. The in situ WAXS measurements are carried out on the D2AM beamline of the European Synchrotron Radiation Facility (ESRF). The X-rays wavelength is 1.54 Å. The cyclic tensile tests are performed at room temperature (21 °C) and low strain rate ($\dot{\lambda} = 4.2 \times 10^{-3}$ s^{-1}) to avoid self-heating. The nominal stretching ratio λ, defined as the sample length l divided by l_0, is measured by videoextensometry. The two-dimensional (2D) WAXS patterns are recorded by a CCD camera (Princeton Instrument). The beam size is small enough (300 μm × 300 μm) to avoid superimposition with the scattered signal. The background, (i.e., air scattering and direct beam intensities) is properly measured in absence of any sample. It can then be subtracted to the total intensity scattered in the presence of the rubber sample. The corrected scattering intensity is finally normalized by the thickness and the absorption of the sample. Each scattering pattern is integrated azimuthally. The deconvolution of the curve $I = f(2\theta)$ enables the extraction of the intensity at the peak top and the width at half height of each crystalline peak and the intensity at the peak top of the amorphous phase. The crystallinity index CI is then determined as follows:[49]

$$\mathrm{CI} = \frac{I_{a0} - I_{a\lambda}}{I_{a0}} \quad (1)$$

where I_{a0} and $I_{a\lambda}$ are the intensities of the amorphous phase at the peak top in the unstretched state and the stretched state, respectively. To our opinion, this method is the most appropriate one to evaluate the absolute crystallinity in the sample because CI does not depend on the estimate of the crystalline peaks area, which can be strongly attenuated or even be in extinction position.

The average crystallite sizes L_{hkl} (L_{200}, L_{102}, and L_{002}) in the direction normal to the (hkl) planes, are estimated from the Scherrer equation:

$$L_{hkl} = \frac{K\lambda_w}{\beta_{1/2}\cos\theta} \quad (2)$$

where λ_w is the wavelength and θ is the Bragg angle. In this study, each crystalline peak is fitted with a Lorentzian function in which the width at half-height is $\beta_{1/2}$. According to the fitted parameters, the K value is 0.64.[50] In order to observe the (002) plane diffraction, the tensile test machine is tilted by an angle around 10°.

3. RESULTS

3.1. Analysis of the SIC Phenomenon. The behavior of the vulcanized NR stretched from $\lambda = 1$ to 6 and then unloaded is first reported. The crystallinity index, the size of the crystallites in the three main directions (L_{200}, L_{120}, L_{002}), and the average number of crystallites per unit of volume are displayed on Figures 1, 2, and 3 respectively.

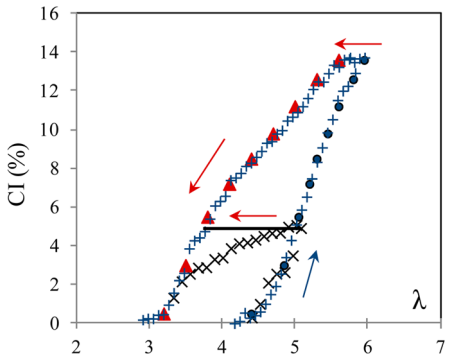

Figure 1. CI versus the stretching ratio during cyclic deformations with maxima at $\lambda = 5.1$ (cross symbol) and $\lambda = 6$ (plus symbols). Cumulative values of CI obtained by discretization used for the model are presented in filled symbols (circles for loading and triangles for unloading). The arrows indicate the direction of the cycles. Horizontal line shows the CI evolution predicted by the model after stretching at $\lambda = 5.1$ and $\lambda = 6$.

The crystallinity index curve (Figure 1) shows a classical trend: the crystallinity appears upon stretching for a critical stretching ratio $\lambda_c = 4.3$ and CI reaches a maximum value of 14% at $\lambda = 6$. During unloading, the crystallites melt. This process is completed at λ_m equal to 3.2. Figure 1 also presents the result for a sample stretched up to 5.1, and then retracted. It can be noted that the loading curves are superimposed and the unloading curves merge when $\lambda \sim 3.5$, i.e., before the melting of all crystallites. At a given stretching ratio, the two CI curves exhibit an hysteresis shape with a CI ratio always higher during the unloading than during the loading. A possible explanation is that part of this hysteresis results from a delay of crystallization. Thus, a sample is stretched and kept at the maximum stretching ratio $\lambda_{max} = 6$ during several minutes instead of being retracted, in order to investigate the role of the crystallization growth on

dx.doi.org/10.1021/ma5006843 | Macromolecules XXXX, XXX, XXX–XXX

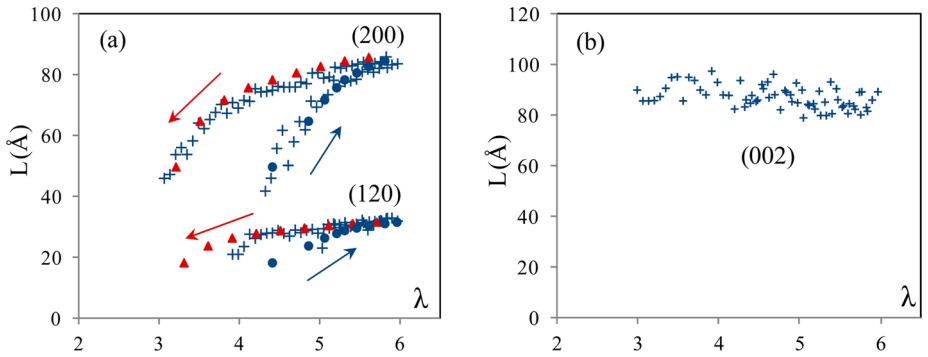

Figure 2. (a) Crystallite sizes L_{200} and L_{120} versus the stretching ratio for the test with λ_{max} = 6 (plus symbols). Filled symbols correspond to the cumulative average crystallite size extracted from discretization. (b) Crystallite size L_{002} versus the stretching ratio. The dotted line is a guide for the eyes.

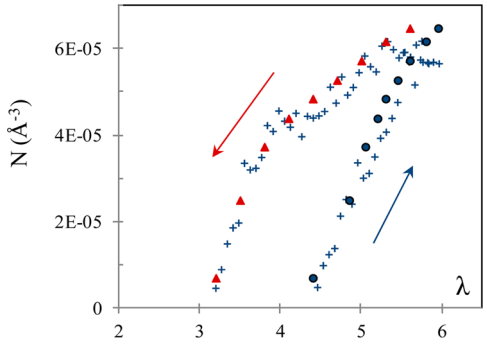

Figure 3. Experimental average number of crystallites per unit of volume (plus symbols) and cumulative number estimated from the model (filled symbols).

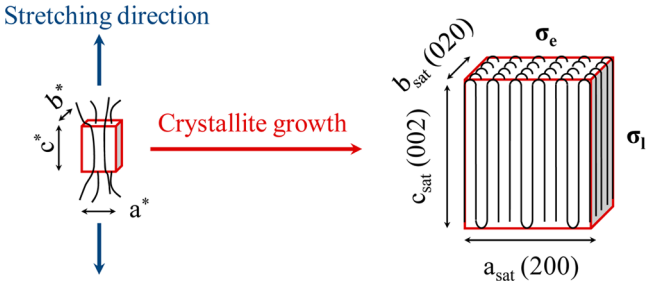

Figure 4. Schematic representation of the SIC from the initial stage at which the nucleus has the necessary critical dimensions for its stability until the end of the growth process where the crystallite reaches its saturated dimension. It is assumed that the final crystallite is mainly made of folded chains and that the growth from the nucleus (star symbol) to the saturated dimension is instantaneous compared to the experimental time.

this hysteresis. As already observed by other authors,[36,51] the crystallinity does not significantly evolve over the duration of the experiment (i.e., less than 1% in our case after 5 min spent in the deformed state). Actually, the SIC kinetics has been recently evaluated by stroboscopic experiments[52,53] and "impact tensile tests".[54,55] In these studies, it was shown that, if the stretching ratio is high enough (above 4), the SIC characteristic time is on the order of 10−100 ms, which is much shorter than the range of stretching time of the present experiments. Moreover, no supplementary increase of the average crystallite volume is observed during the relaxation step. Thus, it can be considered that the growth rate and the nucleation rate are large enough for the crystallization to be completed during the stretching step. The delay of crystallization classically observed during temperature-induced crystallization is called supercooling: a nucleation barrier, related to the excess surface energy of the new crystalline phase, must be overcome to enable the growth of the crystallite nuclei. In our case, the crystallization is strain-induced. Consequently the delay of crystallization can be understood as a "superstraining" phenomenon.

According to Bunn,[56] the crystal structure of the polyisoprene is monoclinic (β = 92°). On the basis of the Nyburg's model,[57] Benedetti[58] rather proposed an orthorhombic structure, which space group is *Pbca*. The size of the unit cell is defined by the following parameters: a = 12.54 Å, b = 9.04 Å (perpendicular to the chain axis) and c = 8.29 Å (parallel to the chain axis). Immirzi et al. proposed a model based on the pseudo-orthorhombic (monoclinic) structure,[59] which is consistent with the model of Bunn. In his recent two-dimensional simulation approach, Che et al.[60] reported a monoclinic structure and gave corrections to the unit cell of SIC. The following lattice constants were proposed: a = 13.048 Å, b = 9.391 Å, and c = 8.551 Å. It finally appears that the crystal structure of the polyisoprene chains has not been completely clarified yet. In our paper, only the order of magnitude of the crystal lattice must be kept in mind.

Experimentally, only the crystallite sizes L_{200} (along the direction "a"), L_{002} (along the stretching direction "c"), and L_{120}, are measured. As shown in Figure 2b, L_{002} immediately reaches a value around 90 Å and only slightly decreases down to 85 Å. By considering the error bar (±5 Å), and its weak variations, this size during the cyclic test is considered constant. It is worth noting that the value of L_{002} is close to the ones reported in literature.[22,34] Conversely, L_{200} and L_{120} evolve during the stretching and reach for the highest stretching ratio 86 and 32 Å, respectively.

Several studies reported that, during stretching of unfilled NR up to a λ of 6, the three dimensions of the crystal lattice change by a maximum of 1%.[19,61] In our experiments, we found that the crystal lattice is strained by −0.7%, −0.9%, and 0.4% along the a, b, and c directions, respectively. It is noteworthy that the peak shifts on the diffraction pattern (plotted in 2θ), from which these values are deduced (−0.0017 rad, −0.0033 rad for a and b, respectively), are much lower than the variations of the peak widths from which L_{200} and L_{120} are calculated (−0.0083 rad and −0.013rad, respectively). For this reason, we are confident that the variations of the crystallite dimensions are not an artifact due to a change of the sizes of

dx.doi.org/10.1021/ma5006843 | *Macromolecules* XXXX, XXX, XXX−XXX

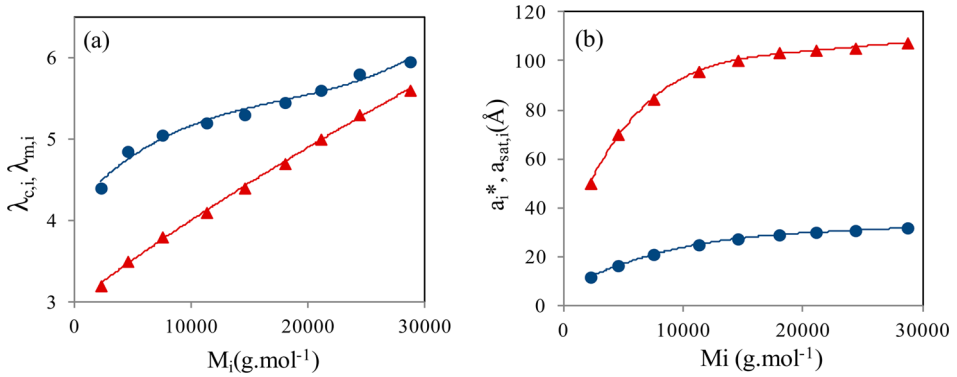

Figure 5. (a) Crystallization stretching ratio (circles) and melting stretching ratio (triangles) of the populations versus their molecular weight. (b) Critical radius (circles) and saturation radius (triangles) of each population involved in the SIC as a function of the corresponding molecular weight. Lines are guides for the eyes.

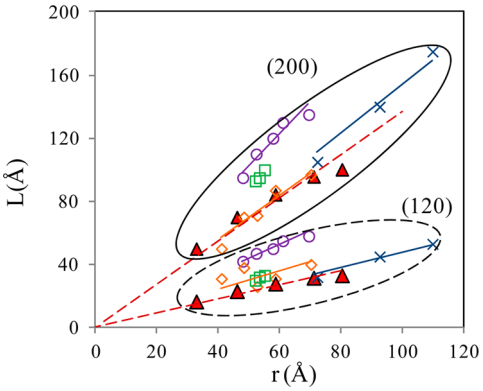

Figure 6. Crystallite size populations $a_{sat,i}$ (200) and $b_{sat,i}$ (120) versus distance between cross-links r_i deduced from the model (filled symbols). Average crystallite sizes L_{200} and L_{120} versus the average distance between cross-links from the literature: ref 37 (cross symbols), ref 19 (circle symbols), and ref 17 (square symbols). Average values measured at $\lambda = 6$ and room temperature from own NR samples (including the NR tested in the present study) are also added (diamond symbols).

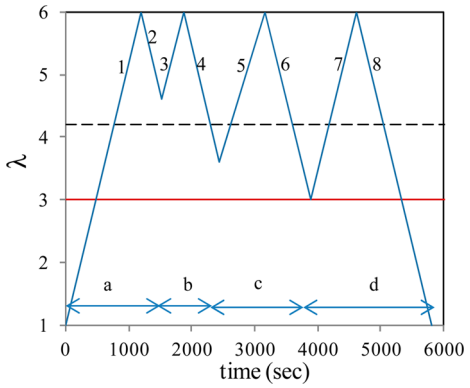

Figure 8. Stretching ratio as a function of the experimental time. The test is made of four cyclic deformations (a, b, c, and d). The maximum stretching ratio is $\lambda = 6$ and the minimum stretching ratio progressively decreases from $\lambda_{min} = 4.6$ to $\lambda_{min} = 1$. Successive loading and unloading phases are numbered from 1 to 8.

the crystal lattice. Note also that the peak shift related to the *c* direction is 7% of the peak width related to L_{002}: this supports our approximation of L_{002} constant with λ.

The ratio between L_{120} and L_{200} is found roughly equal to $^1/_3$, whatever the stretching ratio. This is consistent with previous studies on materials with similar network chain densities.[17,19,37] The increase of the crystallite sizes with stretching ratio is also in agreement with studies on filled and unfilled rubbers[17,62] but in disagreement with other works that report no evolution[63] or a decrease with the stretching ratio.[19,37] Originally, these discrepancies should come from the difficulty to accurately estimate the width at midheight of the crystalline peak when the diffracted intensity is weak. To overcome this limitation, our strategy, consisted in the deconvolution of the WAXS patterns from the higher to the

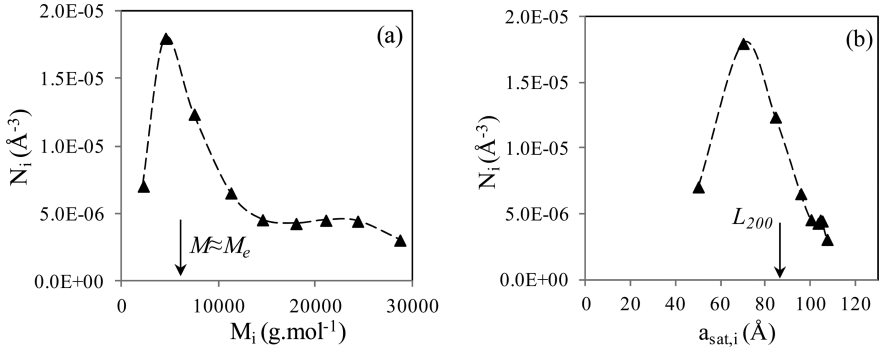

Figure 7. (a) Distribution of the molecular weight M_i and (b) Distribution of the crystallite size populations $a_{sat,i}$ involved in SIC. The arrow indicates the values of the average molecular weight between nodes M (a) and the average saturated size L_{200} (b) at the maximum stretching ratio $\lambda = 6$. The *Y* axis indicates the number density of crystallites of each population estimated from eq 18

dx.doi.org/10.1021/ma5006843 | *Macromolecules* XXXX, XXX, XXX–XXX

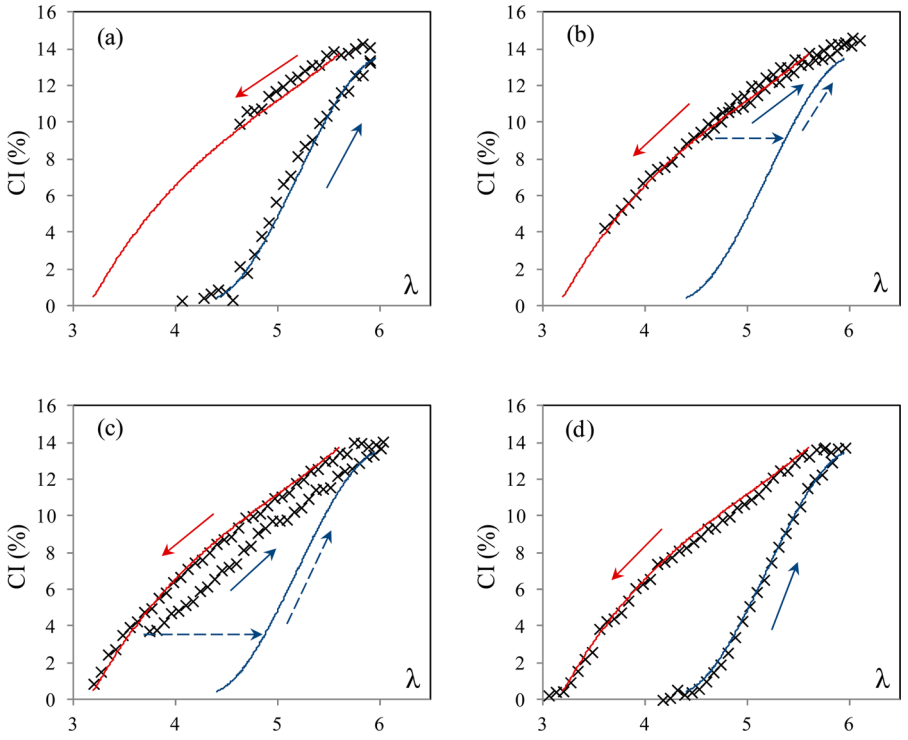

Figure 9. Cyclic deformation after various prestretching. Parts a-d correspond to cycles a−d as defined in Figure 8. Experimental data are given in cross symbols. The continuous lines give the shape of the CI curve used for the model (refer to Figure 1). Continuous arrows indicate the direction of the cycles and dotted arrows the way that should be followed by prediction of the model.

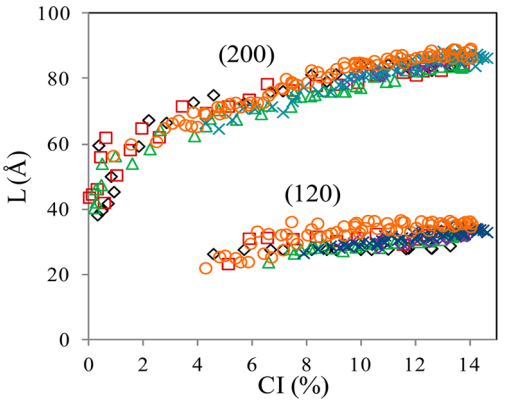

Figure 10. L_{200} and L_{120} as a function of CI for the different cycles: a (diamond symbols), b (cross symbols), c (circle symbols), and d (square symbols).

lower level of crystallinity. Note that even if we are confident on the accuracy of our WAXS analysis, it should be interesting, in a further work, to use the new capabilities of electron microscopy to confirm the values of the crystallite sizes, and to have more insights on their microstructure (chain folding or extended chains).

Similarly to the CI, the size of the crystallites L_{200} and L_{120}, at a given stretching ratio, are found higher upon unloading than upon loading. Note that no morphological change is observed between loading and unloading steps at any given CI. In particular, the relation between the sizes (L_{200} and L_{120}) and CI is not modified. Similar relations are observed for the test carried out at λ_{max} = 5.1 (unpresented data). This suggests that the hysteresis cannot be caused by a morphological change of the crystallites during the unloading step.

From these data, a scenario for SIC is proposed: a nucleus is first created from chains portion aligned in the stretching direction (L_{002}) and the crystallite then grows rapidly up to its final size. To set the order of magnitude, L_{002} corresponds to 22−23 isoprene mers (the distance between two isoprene units is around 4 Å) whereas the average isoprene mers number between two cross-link points in the studied NR is around 100. Since the average distance between adjacent chains is around 6 Å, the maxima values for L_{200} and L_{120} correspond to 14 stacks in the "*a*" direction and 5 stacks in the "*b*" direction.

Moreover, with the angle between the (120) and the (020) directions equal to (19°), the value of L_{020}, is approximated as $0.94L_{120}$. Ultimately, the average volume of the crystallites V_c becomes

$$V_c = L_{200}L_{020}L_{002} = 0.94L_{200}L_{120}L_{002} \quad (3)$$

Under the hypothesis of crystallites with identical dimensions for a given level of stretching ratio, an average number of the crystallites per unit volume N can be deduced:

$$N = \frac{\mathrm{CI}}{V_c} \quad (4)$$

As for the crystallinity index and lengths in the orthogonal directions, the average number of crystallites per unit volume is higher during unloading than loading for a given stretching ratio (Figure 3).

The strong variation of the crystallites number with stretching ratio, the strain rate being slow compared to the nucleation and melting rates, suggests the existence of several crystallite populations. The only possible explanation is the presence of network chain densities heterogeneities. The effect of the average network chain density (ν) on the crystallite sizes is documented in literature: the higher the network chain

dx.doi.org/10.1021/ma5006843 | *Macromolecules* XXXX, XXX, XXX−XXX

density, the lower the crystallite sizes.[17,19,37] The limiting phenomenon for this size is however not clear. Moreover, if the chemical cross-link of the network is homogeneous, Ikeda et al.[64] demonstrated that the higher ν, the lower the stretching ratio at crystallization onset (λ_c). The consequences of the previous assertions on the SIC of a heterogeneously cross-linked network should be the presence of numerous crystallite populations with different sizes. Namely, when the stretching ratio reaches λ_c, the first population appears. The corresponding crystallite size is small because of the high local network chain density of the sample zone where SIC takes place. When the sample is stretched above λ_c, other regions with a lower network chain density reach the critical stretching ratio to induce SIC with crystallites of bigger sizes. Within this frame, the distribution of crystallite populations, their size and the critical stretching ratio at which they appear depend on the heterogeneity of network chain density.

Moreover, during unloading, for the samples stretched at intermediate stretching ratio 5.1, CI decreases only from 5% to 3% prior to reaching the melting curve obtained with λ_{max} equal to 6. The melting point is thus found not to depend on the maximum stretching ratio previously endured by the material. This is consistent with data reported on filled and unfilled rubbers,[18] suggesting that, as for the theoretical frame proposed here, the first crystallites formed during loading are also the last to melt during unloading.

3.2. Thermodynamic Description of Strain-Induced Crystallization. Before considering the different crystallite populations, we first present the classical theory of phase transition adapted to polymers[65] to describe the crystallization of NR. The description is limited to quasi-static testing conditions so that the rate of crystallization is much higher than the strain rate, and the crystals assumed to grow spontaneously (compared to the duration of the experiment) up to its maximum size in the directions orthogonal to the stretching direction, with a constant length along the stretching axis.

The free energy of formation of a crystallite $\Delta\varphi$ with a parallelepipedic shape (Figure 4) is classically written

$$\Delta\varphi = 2c_1(a_1 + b_1)\sigma + 2a_1b_1\sigma_e - a_1b_1c_1\Delta G_m(T, \lambda) \quad (5)$$

where c_1, a_1, and b_1 are the sizes of the crystallites in the directions (002), (200), and (020) respectively. σ and σ_e are the lateral and chain end surface energies.

It is worth noting that the introduction of surface energy is mandatory to enable the description of the superstraining effect. ΔG_m is the melting Gibbs free energy, which at a given stretching ratio λ and temperature T, can be written as follows:

$$\Delta G_m(T, \lambda) = \Delta H_{m,\lambda} - T\Delta S_{m,\lambda} \quad (6)$$

In the literature, the evolution of the crystalline lattice parameters according to λ was found too small to have any influence on the melting enthalpy.[13,66] Consequently, as a first approximation, $\Delta H_{m,\lambda}$ is assumed to be independent of the stretching ratio and named ΔH_m in the following. $\Delta S_{m,\lambda}$ is the entropy of the chains at the stretching ratio λ and is written:

$$\Delta S_{m,\lambda} = \Delta S_{m,1} + \Delta S_{def} \quad (7)$$

where $\Delta S_{m,1}$is the melting entropy of the crystalline phase of an unstretched polymer and ΔS_{def} is the entropy change caused by stretching up to λ.

$\Delta S_{m,1}$ is obtained from the equilibrium state between crystallized and melted chains in the undeformed state ($\Delta G_m = 0$) at $T_{m,\infty}$ (equilibrium melting temperature of the infinite crystal):

$$\Delta S_{m,1} = \frac{\Delta H_m}{T_{m,\infty}} \quad (8)$$

Assuming Gaussian chains behavior for the polymer,[66,67] ΔS_{def} is written:

$$\Delta S_{def} = -\frac{\nu R}{2}\left(\lambda^2 + \frac{2}{\lambda} - 3\right) \quad (9)$$

where ν (mol·cm^{-3}) is the network chain density, R (8.314 J·mol^{-1}·K^{-1}) the constant of ideal gases. Finally, the change of the melting Gibbs free energy of a stretched polymer is

$$\Delta G_m(T, \lambda) = \Delta H_m\left(\frac{T_{m\infty} - T}{T_{m\infty}}\right) + \frac{\nu RT}{2}\left(\lambda^2 + \frac{2}{\lambda} - 3\right) \quad (10)$$

It is worth noting that eq 10 corresponds to the simplified expression of the Gibbs free energy developed by Flory.[12] According to his theory, the crystallite growth should decrease the strain energy of the remaining amorphous part of the chain. Therefore, ν and λ should be affected by the increase of crystallinity. This aspect is not taken into account in our simplified equation. The free energy of crystallization is finally written:

$$\Delta\varphi = 2c_1(a_1 + b_1)\sigma + 2a_1b_1\sigma_e - a_1b_1c_1\left[\Delta H_m\left(\frac{T_{m\infty} - T}{T_{m\infty}}\right) + \frac{\nu RT}{2}\left(\lambda^2 + \frac{2}{\lambda} - 3\right)\right] \quad (11)$$

For NR, $T_{m,\infty}$ is equal to 35.5 °C.[68] The classical Gibbs–Thomson theory considers that thermally induced crystallites are mainly developed in the directions perpendicular to the chain end surface (a_1 and b_1) whereas the dimension c_1 is small. As a result, with σ and σ_e being of the same order, it is generally assumed that $2c_1(a_1 + b_1)\sigma$ is much lower than $2a_1b_1\sigma_e$. From WAXS experiments, the volume of the strain-induced crystallites is found to be more cubic and this assumption is not valid anymore. With the assumption of a strain rate much lower than the rate of crystallization, it can be proposed that crystallites appear when a nucleation barrier has been reached in the three principal directions. This barrier is related to the crystallites surface energy leading to the following equations:

$$\left.\frac{\partial\Delta\varphi}{\partial a_1}\right|_{a_1=a^*,\lambda=\lambda_c} = \left.\frac{\partial\Delta\varphi}{\partial b_1}\right|_{b_1=b^*,\lambda=\lambda_c} = \left.\frac{\partial\Delta\varphi}{\partial c_1}\right|_{c_1=c^*,\lambda=\lambda_c} = 0 \quad (12)$$

$$a^* = \frac{4\sigma}{\Delta G_m(T_c, \lambda_c)}, \quad b^* = a^*, \quad \frac{c^*}{a^*} = \frac{\sigma_e}{\sigma} \quad (13)$$

T_c is the temperature of crystallization, equal to room temperature in this study. The surface energies can be estimated with use of a modified Thomas-Stavley relationship:[69]

$$\sigma = \alpha\Delta H_m(ed)^{1/2} \quad (14)$$

With $\alpha \sim 0.1$for all polymers,[69] $\Delta H_m = 6.1 \times 10^7$ J·m^{-3},[70] e = 0.445 nm, and d = 0.623 nm (d and e correspond to the distance between two polymer chains along b and a

dx.doi.org/10.1021/ma5006843 | Macromolecules XXXX, XXX, XXX–XXX

crystallographic axis respectively). Note that σ_e is almost equal to twice σ in the case of cold crystallization of natural rubber,[32] i.e., for folded chains crystallites. For SIC, it seems reasonable to consider that polymer chains crystallites are first generated from a nucleus of few extended chains from which folded lamella quickly grows. Different arguments plead for such scenario: L_{002} is found stable conversely to the average lateral size of the crystallite, which vary with the stretching level. Second, one must recall that the chains stretching is still relatively low when crystallization occurs (the chain end to end distance is only multiplied by a factor of 4 so that the chains are far from being totally aligned). Finally, the morphology of the strain-induced crystallites is assumed to be mainly of folded chains type, similar to cold crystallization morphology. Consequently, the σ_e/σ ratio is kept equal to 2 and from the Thomas−Stavley relationship, σ is equal to 0.33×10^{-2} J m^{-2} and σ_e to 0.66×10^{-2} J m^{-2}.

During unloading, it is also assumed that before their melting, the crystallites keep their final dimensions (so-called saturated dimensions a_{sat}, b_{sat}, and c_{sat}). The question that arises is the reason for this limited growth. According to Flory (growth model), the crystallite growth is possibly due to a mechanical relaxation of the remaining amorphous part of the chains. Thermodynamically, crystallization can occur because the energy balance is favorable (lower entropic energy). At higher stretching level, a larger number of mers are included into the crystallite. This tends to strongly attenuate the mechanical relaxation and thus explains why crystallite growth is finally stopped. The crystallite growth might also be limited by the presence of cross-links surrounding the crystallites, because of the topological constraint they create.[71] Indeed, during crystallization, cross-links and entanglements originally in the crystallizing phase are gradually repulsed out of the crystallites and accumulated in the crystallite neighborhood. Theoretically, this can be pictured by an increase of the surface energy, and therefore must be accounted for in the equation of the crystallization free energy. Such a development is proposed by Hoffman in his work related to flow induced crystallization in polyethylene systems.[72] Another hypothesis is to consider that this phenomenon does not change the global thermodynamic equilibrium description. This second option is preferred.

Finally, within the proposed framework, the description of strain-induced crystallization is very similar to the one of thermal induced crystallization and the reason for a limited size of the crystallite is not included in the thermodynamic equations. The limiting conditions for the melting of the crystallites are reached when the amorphous and crystalline phases are in equilibrium, i.e., when the free energy of crystallization is equal to zero:

$$\Delta\varphi)_{a_{sat},b_{sat},c_{sat},\lambda_m,T_m} = 0 \tag{15}$$

Finally, the change of the melting Gibbs free energy of a stretched polymer can be deduced using eq 15, and the values of a_{sat}, b_{sat}, and c_{sat} determined experimentally:

$$a_{sat} = \frac{8\sigma}{\Delta G_m(\lambda_m, T_m) - \frac{2\sigma_e}{c_{sat}}}, \quad b_{sat} = \frac{a_{sat}}{3}, \quad c_{sat} = L_{002} \tag{16}$$

The relation between b_{sat} and a_{sat} is an a-priori assumption which is justified by the experiments described above. Equation 16 predicts that for a fixed melting stretching ratio λ_m, high enough to neglect the contribution of the enthalpy term and the chain end surface energy term, the saturation radius a_{sat} should be proportional to the inverse of the network chain density ν. In other words, it should be proportional to the average number of monomers between cross-links $N = \rho/M_0\nu$ with M_0 = 64 g·mol^{-1} the molecular weight of a monomer.

The previous thermodynamic development can describe SIC of a rubber with a homogeneous network chain density ν and therefore a unique crystallite size. In the following paragraph, we propose to extend this description to analyze SIC in rubber in which the network is heterogeneous.

3.3. Determination of Crystallite Populations. As already evoked in the previous sections, it has been widely shown that NR cross-link density is heterogeneous. Thermoporosimetry presented in Appendix and data reported in the literature strongly support this idea. The evolution of the average number of crystallites legitimates the use of several crystallite populations of different sizes to describe SIC of NR. Each population is associated with a specific network chain density. It is characterized by a stretching ratio at crystallization onset $\lambda_{c,i}$, a melting stretching ratio $\lambda_{m,i}$, a critical and a saturated radius, a^*_i and $a_{sat,i}$, respectively. It must be recalled here the empiric relation between the average lateral crystallite sizes: $L_{120} = {}^1/_3 L_{200}$. We assume the same relation for each crystallite population; i.e., $b_{sat,i} = {}^1/_3 a_{sat,i}$. Because L_{002} does not significantly vary during the mechanical cycle, the values $c_{sat,i}$ of the different populations are all assumed equal to L_{002} =85 Å. Even if the strain rate chosen for our experiments is sufficiently low to significantly avoid delay of crystallization, nucleation and growth are intrinsically kinetic phenomena. Conversely, melting seems poorly strain rate dependent as recently shown by Brüning.[55] Consequently, we propose that the melting profile should be *a priori* the most adapted curve for a thermodynamic description of SIC. The distribution of the population is obtained thanks to a discretization of the melting curves giving the crystallinity and the length of the crystallites L_{200} as a function of the stretching ratio during unloading (filled data points in Figure 1 and 2). The discretization of the sizes L_{120} is a hard task because of its low values. They are deduced from the discretized values of L_{200} by applying the factor of 1/3, as previously discussed. The stretching ratio increment $\Delta\lambda_m$ is chosen equal to 0.3 so that the melting curves of Figure 1 can be described by 9 populations. The discretization procedure also assumes that the local stretching ratio of the chains involved in the population i is equal to the macroscopic deformation $\lambda_{c,i}$. mechanically, this means a parallel combination of these populations, i.e., a cocontinuous arrangement. A serial/parallel model is probably more appropriate, but is not developed in the present paper in order to keep a simple analytical approach.

The crystallite characteristic extracted from WAXS measurements are necessarily averaged, as discussed above. CI_i, N_i and V_i are the values of CI, N and V related to a given population *i*. Such values are incrementally deduced from the knowledge of the characteristics of the population $i - 1$:

$$CI_i = CI - \sum_{i-1}^{j=1} CI_j; \quad i > 1 \tag{17}$$

$$N_i = N - \sum_{i-1}^{j=1} N_j; \quad i > 1 \tag{18}$$

dx.doi.org/10.1021/ma5006843 | Macromolecules XXXX, XXX, XXX−XXX

$$V_i = \frac{CI_i}{N_i} \tag{19}$$

The most thermodynamically stable population is the first formed during loading (i.e., the first to reach the necessary superstraining state) and the last to melt during unloading. Its crystalline fraction corresponds to the experimentally measured CI and its size corresponds to the size measured by WAXS. This, in turn, enables to deduce the volume V_1 of the crystallites and therefore their number N_1.

ν_i involved in the considered population can been deduced from

$$\nu_i = \frac{\frac{16\sigma}{a_{sat,i}} + \frac{4\sigma_e}{c_{sat,i}} + \frac{2\Delta H_m \Delta T}{T_{m,\infty}}}{RT\left(\lambda_{m,i}{}^2 + \frac{2}{\lambda_{m,i}} - 3\right)} \tag{20}$$

The elastically effective network chain density ν_i is related to chemical cross-links but also trapped entanglements. Because of the slow strain rate used in our study, it is reasonable to neglect the contribution of the free entanglements in the SIC process. M_i is thus defined as the molecular weight between chemical cross-links and trapped entanglements:

$$M_i = \frac{\rho}{\nu_i} \tag{21}$$

With ρ = 0.92 g·cm^{-3}. From the knowledge of ν_i and λ_i, a critical radius a_i* can be deduced:

$$a_i^* = \frac{4\sigma}{\Delta G_m(T_{c,i}, \lambda_{c,i}, \nu_i)} \tag{22}$$

Parameters deduced from the above calculations are plotted against the molecular weight M_i of each population in Figure 5, parts a and b. $\lambda_{c,i}$ and $\lambda_{m,i}$ increase with M_i. The first crystallites that appear are made of short chains. The crystallites made of long chains crystallize at larger λ_{ci}, are the largest, thermodynamically less stable, and melt first during unloading. Note that this is the opposite of what is generally observed in thermal crystallization, where the smallest crystallites melt first.

Figure 5b also shows that the critical radius a_1* increases with the molecular weight. The smallest one (first crystallite size population) is found to be equal to 12 Å. From eq 13, b_1* is equal to 12 Å and c_1* to 24 Å. Within the theoretical frame used here, strain-induced crystallization of natural rubber is initiated from nucleus whose size is in the range of the crystal lattice. This is in agreement with previous works related to thermally generated crystallites of natural rubber.[71,73] In addition, the molecular weight M_i of the elastically effective network chains involved in the first crystallites population is around 2200 g·mol^{-1}. This value is 3 times lower than the average molecular weight of the elastically effective network chains deduced from swelling ($M \approx 6500$ g·mol^{-1}).

The calculated saturated radius $a_{sat,i}$ increases with M_i. As discussed above (see eq 16), this result is almost intuitive considering a homogeneous network. In the model, this saturation radius is experimentally related to both melting stretching ratio and network chain density. It increases with increase of the first parameter but decreases with the second one. The variations of $\lambda_{m,i}{}^2$ (for λ_m varying from 3.2 to 5.6) are weaker than the ones of the density ν_i (from 2200 to 27000 g·mol^{-1} in molecular weight units). Hence, the network chain density is finally the predominant parameter that controls both the nucleation and the size of the crystallites.

The values of $a_{sat,i}$ and $b_{sat,i}$ for the five first populations (i.e., before the saturation of the values a_{sat}, cf. Figure 5b) are now plotted as a function of the distance between cross-links r_i. Following Trabelsi et al.,[37] the r_i value for unstretched chains can be deduced from the relation $r_i = 0.8(\rho/\nu_i)^{1/2}$, with ρ the rubber density (in g mol^{-1}). A linear evolution is found between the saturation sizes and r_i (see Figure 6). The average sizes of the crystallites reported in the literature are added to the plot. For all these works, SIC is analyzed during cyclic deformation at room temperature performed in the same range of strain rate as the one of ours. The extracted values of average crystallite sizes in the directions (200) and (120) are all measured at the maximum stretching ratio of the loading. Besides, the average network chain densities of the samples tested have been estimated thanks to swelling in toluene and from the Flory−Rehner equation, similarly to the protocol followed in our study. As shown in Figure 6, linear evolutions are found with slopes varying from 1.39 to 2.04 for L_{200} and from 0.48 to 0.87 for L_{120}. The data are in good agreement with our model prediction, suggesting that the crystallite sizes and network chain densities distributions are realistic as they cover the range of average values from literature. The present methodology has also been successfully applied to other vulcanized rubbers with different average network chain densities and again shows very similar correlations between the size of the crystallites and the distance between nodes (linear fit with similar slope factors, with a very close distribution for all samples).

N_i is now plotted as a function of the molecular weight M_i (Figure 7a) and as a function of the crystallite size (Figure 7b). Both distributions are centered on the very first populations. Despite their small sizes, the large number of crystallites in the first populations suggests that the smallest crystallites are finally the main contributors to SIC. The distribution broadens at higher molecular weight. The large molecular weight of the last populations, up to 4 times higher than the average molecular weight M deduced from swelling measurements (6500 g·mol^{-1}), suggests that the network density distribution is highly broad. This observation is in agreement with thermoporosimetry experiment (refer to Figure 11 in the Appendix).

Using the parameters deduced from the experimental data with a maximum stretching ratio of 6, the CI−λ curve for cycle with a maximum stretching ratio of 5.1 is calculated and plotted on Figure 1. Obviously, the stretching part is superimposed to the experimental data since these ones are superimposed to the data obtained with λ_{max} equal to 6. For the melting curve, the model however predicts a plateau while the experimental data show a slight decrease of CI before it reaches the reference melting curve. This slight discrepancy has likely its origin in the strong assumptions of the model. Each crystallite population is assumed to be stabilized at its maximum value, and this saturated size is assumed to be independent of the stretching level, until the stretching ratio below which it can melt is reached. Nevertheless, the maximum stretching ratio might influence the global final size distribution of the crystallite, at least for the largest populations.

3.4. Cyclic Deformation from Different Prestretched States. A NR sample is now cyclically deformed several times up to the same final stretching ratio λ_{max} equal to 6. The test is carried out at room temperature and slow strain rate. The specificity of this test is that the minimum stretching ratio

dx.doi.org/10.1021/ma5006843 | Macromolecules XXXX, XXX, XXX−XXX

reached during unloading progressively decreases with the cycle number. The mechanical history of this test is summarized in Figure 8.

Figure 9 presents the evolution of CI during the different cycles (a−d). For the first cycle in the prestretched state (so-called cycle b), the cyclic deformation only exhibits weak crystallinity hysteresis. A higher hysteresis is found for cycle c. At the end of the cycle c, all the crystallites have melted and the crystallinity exhibits the classical hysteresis (cycle d). Note that all the melting curves are superimposed to the one obtained with the unique cycle presented in the previous parts. This result shows that no cumulative effect is observed on CI by addition of cycles carried out above the melting stretching ratio λ_m. In particular, if the final stretching ratio reached during such cycles does not exceed the maximum stretching ratio of 6, prestretching the sample does not affect the shape of the melting curve. Consequently, it supports the choice of the initial melting curve, as a reference for the discretization of the crystallite populations.

Average size of the crystallites is also studied (Figure 10). The relation between CI and the average size of the crystallites in the three main directions is independent of the different cycles and exhibits a unique curve. Thus, the application of various prestretching has no influence on the strain-induced crystallization measured at the maximum stretching ratio (with the slow strain rate used for these experiments): the crystallite populations successively melt and recrystallize to finally provide the same crystalline state at the maximum stretching ratio. The model would predict that the populations melted during partial unloading should only renucleate if the critical stretching ratio is reached again during loading. Consequently, within this scenario, plateaux should have been observed for loading phases of cycles b and c (namely phases 3 and 5), as illustrated by dotted arrows in Figure 9. Within the frame of the model the only explanation is the following: if the macromolecules have not totally relaxed during unloading (this is likely since the material is still stretched), renucleation can be eased, suggesting a memory effect of the chains alignment.

These new results emphasize the necessity to pursue experimental investigations in order to better understand and describe SIC of NR. From an experimental point of view, it also shows that the crystallinity index during a fatigue test can be estimated from the melting curve alone, as far as the minimum stretching ratio is not too close from the one needed for a complete melting.

4. CONCLUSION

From the observation of in situ wide angle X-rays scattering (WAXS) performed during a cyclic test at slow strain rate, a scenario for strain-induced crystallization (SIC) of natural rubber (NR) is proposed. The presence of different crystallite populations related to different network chain densities in the material is assumed. The crystallization is thought to be the result of the progressive nucleation and instantaneous growth of these populations. Following these ideas, a model is developed to describe both the crystallization and the melting curves (i.e., the crystallinity index and the crystallite size as a function of the stretching ratio). From this description, the size of the crystallite populations increases and the network chain density associated with them decreases when the stretching ratio increases. Additional original cyclic experiments performed above λ_m also evidence that, even after their melting, the chains of the crystallites keep the memory of their alignment (as far as the stretching ratio has not been decreased down to λ_m) and ease the renucleation process during reloading.

APPENDIX

Thermoporosimetry experiments: samples are put into a solvent (cyclohexane) during 3 days in order to reach the swelling equilibrium. They are then extracted and put into an aluminum crucible. The melting behavior of the solvent in the samples is studied using a PerkinElmer Pyris diamond DSC (differential scanning calorimetry). First, the sample is cooled down to −50 °C at 10 °C/min followed by an isothermal step at −50 °C for 2 min. Finally, the sample is heated at 10 °C/min up to +30 °C. The melting curve is given in Figure 11. The first peaks that appear during heating correspond to the melting of the cyclohexane entrapped in the network. The last peak (around 3 °C) corresponds to the melting point of free cyclohexane (i.e., in excess). Melting peaks are deconvoluted by use of asymmetric Lorentzian functions. The broad distribution of the melting temperature certainly attests for the large distribution of the chain length between cross-links.

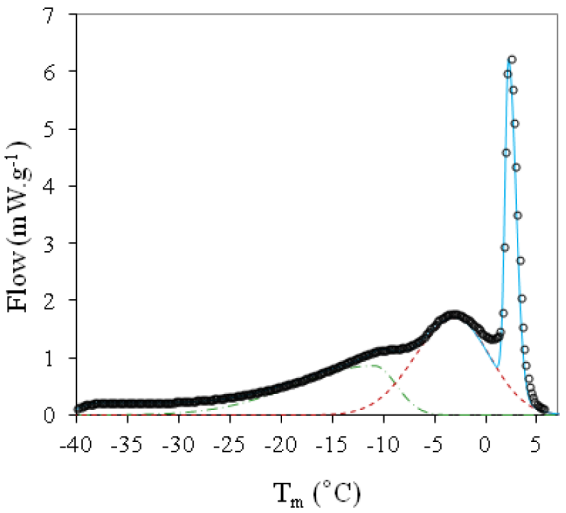

Figure 11. Melting curve of NR sample normalized by the weight of the sample. Melting peaks deconvoluted with Lorentzian functions (dotted lines for peaks of the cyclohexane entrapped in the network and solid line for free cyclohexane).

AUTHOR INFORMATION

Corresponding Author

*(L.C) E-mail: laurent.chazeau@insa-lyon.fr. Telephone: +33 (0) 4 72438357. Fax: +33 (0) 4 72438528.

Notes

The authors declare no competing financial interest.

ACKNOWLEDGMENTS

The authors are indebted to the European Synchrotron Radiation Facility (ESRF) and the local contact Dr. C. Rochas for providing the necessary beamline time and technical assistance in the experiments on the D2AM line.

REFERENCES

(1) Trabelsi, S.; Albouy, P. A.; Rault, J. *Macromolecules* **2002**, *35* (27), 10054−10061.

(2) Le Cam, J. B.; Toussaint, E. *Macromolecules* **2010**, *43* (10), 4708−4714.
(3) Rublon, P.; Huneau, B.; Saintier, N.; Beurrot, S.; Leygue, A.; Verron, E.; Mocuta, C.; Thiaudiere, D.; Berghezan, D. *J. Synchrot. Radiat.* **2013**, *20*, 105−109.
(4) Brüning, K.; Schneider, K.; Roth, S. V.; Heinrich, G. *Polymer* **2013**, *54* (22), 6200−6205.
(5) Rublon, P.; Huneau, B.; Verron, E.; Saintier, N.; Beurrot, S.; Leygue, A.; Mocuta, C.; Thiaudiere, D.; Berghezan, D. *Eng. Fract. Mech.* **2014**, *123*, 59−69.
(6) Beurrot-Borgarino, S.; Huneau, B.; Verron, E.; Rublon, P. *Int. J. Fatigue* **2013**, *47*, 1−7.
(7) Saintier, N.; Cailletaud, G.; Piques, R. *Mater. Sci. Eng. A: Struct. Mater. Prop. Microstruct. Process.* **2011**, *528* (3), 1078−1086.
(8) Munoz, L.; Vanel, L.; Sanseau, O.; Sotta, P.; Long, D.; Guy, L.; Odoni, L. *Key Eng. Mater.* **2011**, *1382* (488), 666.
(9) Katz, J. R. *Naturwissenschaften* **1925**, *13*, 410−416.
(10) Yeh, G. S. Y.; Hong, K. Z. *Polym. Eng. Sci.* **1979**, *19* (6), 395−400.
(11) Gaylord, R. J.; Lohse, D. J. *Polym. Eng. Sci.* **1976**, *16* (3), 163−167.
(12) Flory, P. J. *J. Chem. Phys.* **1947**, *15* (6), 397−408.
(13) Alfrey, T.; Mark, H. *J. Phys. Chem.* **1942**, *46* (1), 112−118.
(14) Poshtan, E. A.; Dargazany, R.; Itskov, M. *Proc. Appl Math. Mech.* **2011**, *11* (1), 423−424.
(15) Tosaka, M.; Kohjiya, S.; Ikeda, Y.; Toki, S.; Hsiao, B. S. *Polym. J.* **2010**, *42* (6), 474−481.
(16) Ikeda, Y.; Yasuda, Y.; Hijikata, K.; Tosaka, M.; Kohjiya, S. *Macromolecules* **2008**, *41* (15), 5876−5884.
(17) Chenal, J. M.; Chazeau, L.; Guy, L.; Bomal, Y.; Gauthier, C. *Polymer* **2007**, *48* (4), 1042−1046.
(18) Albouy, P. A.; Marchal, J.; Rault, J. *Eur. Phys. J. E* **2005**, *17* (3), 247−259.
(19) Tosaka, M.; Murakami, S.; Poompradub, S.; Kohjiya, S.; Ikeda, Y.; Toki, S.; Sics, I.; Hsiao, B. S. *Macromolecules* **2004**, *37* (9), 3299−3309.
(20) Toki, S.; Sics, I.; Ran, S. F.; Liu, L. Z.; Hsiao, B. S. *Polymer* **2003**, *44* (19), 6003−6011.
(21) Choi, I. S.; Roland, C. M. *Rubber Chem. Technol.* **1997**, *70* (2), 202−210.
(22) Yeh, G. S. Y. *Polym. Eng. Sci.* **1976**, *16* (3), 138−144.
(23) Luch, D.; Yeh, G. S. Y. *J. Macromol. Sci.—Phys. B* **1973**, *7* (1), 121−155.
(24) Huneau, B. *Rubber Chem. Technol.* **2011**, *84* (3), 425−452.
(25) Tosaka, M. *Polym. J.* **2007**, *39* (12), 1207−1220.
(26) Martinez, J. R. S.; Le Cam, J. B.; Balandraud, X.; Toussaint, E.; Caillard, J. *Polymer* **2013**, *54* (11), 2727−2736.
(27) Martinez, J. R. S.; Le Cam, J. B.; Balandraud, X.; Toussaint, E.; Caillard, J. *Polymer* **2013**, *54* (11), 2717−2726.
(28) Mitchell, J. C.; Meier, D. J. *J. Polym. Sci., Part A2: Polym. Phys.* **1968**, *6* (10PA), 1689.
(29) Goritz, D.; Grassler, R. *Rubber Chem. Technol.* **1987**, *60* (2), 217−226.
(30) Miyamoto, Y.; Yamao, H.; Sekimoto, K. *Macromolecules* **2003**, *36* (17), 6462−6471.
(31) Yeh, G. S. Y. *Polym. Eng. Sci.* **1976**, *16* (3), 145−151.
(32) Edwards, B. C. *J. Polym. Sci., Part B: Polym. Phys.* **1975**, *13* (7), 1387−1405.
(33) Luch, D.; Yeh, G. S. Y. *J. Appl. Phys.* **1972**, *43* (11), 4326−4338.
(34) Andrews, E. H. *J. Polym. Sci., Part A2: Polym. Phys.* **1966**, *4* (4PA2), 668.
(35) Tsuji, M.; Shimizu, T.; Kohjiya, S. *Polym. J.* **1999**, *31* (9), 784−789.
(36) Toki, S.; Sics, I.; Hsiao, B. S.; Tosaka, M.; Poompradub, S.; Ikeda, Y.; Kohjiya, S. *Macromolecules* **2005**, *38* (16), 7064−7073.
(37) Trabelsi, S.; Albouy, P. A.; Rault, J. *Macromolecules* **2003**, *36* (20), 7624−7639.
(38) Toki, S.; Fujimaki, T.; Okuyama, M. *Polymer* **2000**, *41* (14), 5423−5429.
(39) Rao, I.; Rajagopal, K. *Int. J. Solids Struct.* **2001**, *38* (6), 1149−1167.
(40) Suzuki, T.; Osaka, N.; Endo, H.; Shibayama, M.; Ikeda, Y.; Asai, H.; Higashitani, N.; Kokubo, Y.; Kohjiya, S. *Macromolecules* **2010**, *43* (3), 1556−1563.
(41) Ikeda, Y.; Higashitani, N.; Hijikata, K.; Kokubo, Y.; Morita, Y.; Shibayama, M.; Osaka, N.; Suzuki, T.; Endo, H.; Kohjiya, S. *Macromolecules* **2009**, *42* (7), 2741−2748.
(42) Toki, S.; Hsiao, B. S. *Macromolecules* **2003**, *36* (16), 5915−5917.
(43) Vieyres, A.; Pérez-Aparicio, R.; Albouy, P.-A.; Sanseau, O.; Saalwächter, K.; Long, D. R.; Sotta, P. *Macromolecules* **2013**, *46* (3), 889−899.
(44) Valentin, J. L.; Posadas, P.; Fernandez-Torres, A.; Malmierca, M. A.; Gonzalez, L.; Chasse, W.; Saalwachter, K. *Macromolecules* **2010**, *43* (9), 4210−4222.
(45) Qin, Q.; McKenna, G. B. *J. Polym. Sci., Part B: Polym. Phys.* **2006**, *44* (24), 3475−3486.
(46) Tosaka, M. *Macromolecules* **2009**, *42* (16), 6166−6174.
(47) Rauline, R. U.S. Patent 5,227,425, (Michelin), 1993.
(48) Flory, P. J.; Rehner, J. *J. Chem. Phys.* **1943**, *11* (11), 521−526.
(49) Mitchell, G. R. *Polymer* **1984**, *25* (11), 1562−1572.
(50) Trabelsi, S. Ph.D. Thesis, Université Paris Sud 11, Orsay, France, 2002.
(51) Rault, J.; Marchal, J.; Judeinstein, P.; Albouy, P. A. *Eur. Phys. J. E* **2006**, *21* (3), 243−261.
(52) Candau, N.; Chazeau, L.; Chenal, J. M.; Gauthier, C.; Ferreira, J.; Munch, E.; Rochas, C. *Polymer* **2012**, *53* (13), 2540−2543.
(53) Albouy, P. A.; Guillier, G.; Petermann, D.; Vieyres, A.; Sanseau, O.; Sotta, P. *Polymer* **2012**, *53* (15), 3313−3324.
(54) Tosaka, M.; Senoo, K.; Sato, K.; Noda, M.; Ohta, N. *Polymer* **2012**, *53* (3), 864−872.
(55) Bruning, K.; Schneider, K.; Roth, S. V.; Heinrich, G. *Macromolecules* **2012**, *45* (19), 7914−7919.
(56) Bunn, C. W. *Proc. R. Soc. London A: Math. Phys. Sci.* **1942**, *180* (A980), 0040−0066.
(57) Nyburg, S. *Acta Crystallogr.* **1954**, *7* (5), 385−392.
(58) Benedetti, E.; Corradini, P.; Pedone, C. *Eur. Polym. J.* **1975**, *11* (8), 585−587.
(59) Immirzi, A.; Tedesco, C.; Monaco, G.; Tonelli, A. E. *Macromolecules* **2005**, *38* (4), 1223−1231.
(60) Che, J.; Burger, C.; Toki, S.; Rong, L.; Hsiao, B. S.; Amnuaypornsri, S.; Sakdapipanich, J. *Macromolecules* **2013**, *46* (11), 4520−4528.
(61) Poompradub, S.; Tosaka, M.; Kohjiya, S.; Ikeda, Y.; Toki, S.; Sics, I.; Hsiao, B. S. *J. Appl. Phys.* **2005**, *97* (10), 103529-1−103529-9.
(62) Chenal, J. M.; Gauthier, C.; Chazeau, L.; Guy, L.; Bomal, Y. *Polymer* **2007**, *48* (23), 6893−6901.
(63) Beurrot-Borgarino, S. Thesis. Ecole centrale de nantes-ECN, Nantes, France, 2012.
(64) Ikeda, Y.; Yasuda, Y.; Makino, S.; Yamamoto, S.; Tosaka, M.; Senoo, K.; Kohjiya, S. *Polymer* **2007**, *48* (5), 1171−1175.
(65) Sperling, L. H. *Introduction to physical polymer science*; Wiley: New York, 2005.
(66) James, H. M.; Guth, E. *J. Chem. Phys.* **1943**, *11* (10), 455−481.
(67) Treloar, L. R. G. *The physics of rubber elasticity*; Oxford: Oxford, U.K., 1975.
(68) Dalal, E. N.; Taylor, K. D.; Phillips, P. J. *Polymer* **1983**, *24* (12), 1623−1630.
(69) Hoffman, J.; Davis, G.; Lauritzen, J.; Jr.; Plenum Press: New York, 1976.
(70) Kim, H. G.; Mandelke, L. *J. Polym. Sci., Part A2: Polym. Phys.* **1972**, *10* (6), 1125.
(71) Gent, A. N. *Trans. Faraday Soc.* **1954**, *50* (5), 521−533.
(72) Hoffman, J. D. *Polymer* **1979**, *20* (9), 1071−1077.
(73) Andrews, E. H.; Owen, P. J.; Singh, A. *Proc. R. Soc. London A: Math. Phys. Sci.* **1971**, *324* (1556), 79.